A Control Scheme for the Reduction of Thruster-Manipulator Interactions in Space Robotic Systems

E. Martin[1]   E. Papadopoulos[2]   J. Angeles[1]

[1]Department of Mechanical Engineering and Centre for Intelligent Machines,
McGill University, Montreal, Quebec, Canada, H3A 2K6

[2]Department of Mechanical Engineering,
National Technical University of Athens, 15773 Athens, Greece

Abstract

Space manipulators mounted on an on-off thruster-controlled base are envisioned to assist in the assembly and maintenance of space structures. When handling large payloads, manipulator joint and link flexibility become important, for they can result in payload-attitude controller fuel-replenishing dynamic interactions. In this paper, the dynamics model of an N-flexible-joint space manipulator is developed. The model of a three-flexible-joint manipulator mounted on a six-degree-of-freedom spacecraft is used to compare three different on-off thruster attitude control systems. Two variations of a classical control scheme are suggested to minimize such undesirable dynamic interactions, as well as thruster fuel consumption.

1 Introduction

Robotic devices in orbit will play an important role in space exploration and exploitation. Their mobility can be enhanced by mounting them on free-flying bases, controlled by on-off thrusters. Such robots introduce a host of dynamic and control problems not found in terrestrial applications. When handling large payloads, manipulator joint or structural flexibility becomes important and can result in payload-attitude controller fuel-replenishing dynamic interactions. Such interactions may lead to control system instabilities, or manifest themselves as limit cycles [1].

The CANADARM-Space Shuttle system is the only operational space robotic system to date. Its Reaction Control System (RCS), which makes use of on-off thrusters, is designed assuming rigid-body motion, and using single-axis, thruster switching logic based on phase-plane techniques. This approach is common in the design of thruster-based control systems. However, the flexible modes of this space robotic system have rather low frequencies, which continuously change with manipulator configuration and payload, and can be ex-cited by the RCS activity. The performance degradation of the RCS due to the deployment of a flexible *payload*, with or without the CANADARM, has been studied in [2]. A new design for the RCS was developed to reduce the impact of large measurement uncertainties in the rate signal during attitude control, thereby increasing the performance of the RCS for rigid-body motion [3]. However, the flexibility problem was not addressed. Currently, the method for resolving these problems consists of performing extensive simulations. If dynamic interactions occur, corrective actions are taken, which would include adjusting the RCS parameter values, or simply changing the operational procedures [2]. The consequences of such interactions can be problematic, since fuel is a scarce resource in space; hence, classical attitude controllers must be improved to reduce the possibility of such dynamic interactions.

This interaction problem was studied using a single-mode, linear translational mechanical system to approximate the dynamic behaviour of a two-flexible-joint manipulator mounted on a three-degree-of-freedom (dof) base with a constant system damping ratio [4], and with a variable one [5]. A state-estimator and design guidelines were suggested to minimize such undesirable dynamic interactions, as well as thruster fuel consumption. These results were validated in [6] using a more realistic model with rotational degrees of freedom. In this paper, a general technique to model a space manipulator with flexible joints is first developed and two variations of a classical control scheme are suggested that reduce the undesirable effects of dynamic interactions, as well as thruster fuel consumption.

2 System Description
2.1 Dynamics Modelling

In this subsection, the dynamics model of an N-flexible-joint space manipulator is obtained using a Lagrangian approach. Since the time scale of robotic mo-

tions are assumed to be relatively small compared to the orbital period, orbital mechanics effects are neglected. The kinematics of the free-flying space manipulator is expressed using the spacecraft centre of mass (CM) C as a reference point to describe system translation. The inertial position vector of an arbitrary point P of the system, $\mathbf{p}$, can be written as

$$\mathbf{p} = \mathbf{c} + \boldsymbol{\rho}, \qquad \text{with} \qquad \boldsymbol{\rho} = \mathbf{c}_i + \mathbf{p}_i \qquad (1)$$

where $\mathbf{c}$, $\boldsymbol{\rho}$, $\mathbf{c}_i$, and $\mathbf{p}_i$ are, respectively, the position vectors of C, of point P with respect to C, the CM C_i of the i-th body with respect to the spacecraft CM, and of point P with respect to the i-th body CM, see Fig. 1.
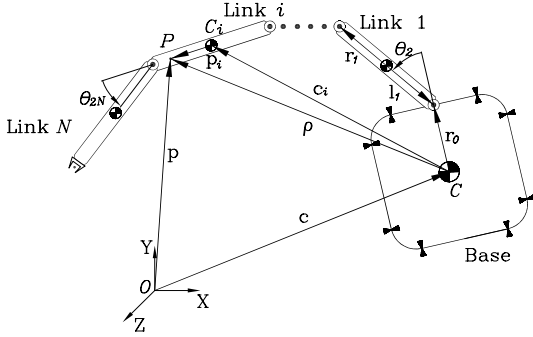

Figure 1: A space manipulator system

Now, vectors $\boldsymbol{\theta}_a = [\theta_1, \theta_3, \cdots, \theta_{2N-1}]^T$ and $\boldsymbol{\theta}_n = [\theta_2, \theta_4, \cdots, \theta_{2N}]^T$ are defined as the rotor-joint variables and the link-joint variables, at the joints, respectively. Here, subscripts a and n stand for the actuated and non-actuated variables. These two vectors are not the same due to joint flexibility. Assuming lumped flexibility at the joints, links are considered rigid and the kinetic energy expression of the system is given by

$$T = \frac{1}{2} \int_M \dot{\mathbf{p}} \cdot \dot{\mathbf{p}} \, dM + \frac{1}{2} \dot{\boldsymbol{\theta}}_a^T \mathbf{J} \dot{\boldsymbol{\theta}}_a \qquad (2)$$

where M is the total mass of the system, and $\mathbf{J}$ is the moment-of-inertia matrix of the rotors.

For a free-flyer, microgravity effects are very small compared to control forces, and hence, they are neglected. Thus, the potential energy is only due to joint elasticity. Moreover, viscous friction forces due to damping can be taken into account using Rayleigh's dissipation function R. We thus have,

$$V = \frac{1}{2} \Delta \boldsymbol{\theta}^T \mathbf{K}_r \Delta \boldsymbol{\theta}, \qquad R = \frac{1}{2} \Delta \dot{\boldsymbol{\theta}}^T \mathbf{C}_r \Delta \dot{\boldsymbol{\theta}} \qquad (3)$$

where $\mathbf{K}_r$ is a stiffness matrix defined as $\mathbf{K}_r = \text{diag}(k_1, k_2, \cdots, k_N)$, $\mathbf{C}_r$ is a damping matrix defined as $\mathbf{C}_r = \text{diag}(c_1, c_2, \cdots, c_N)$, while $\Delta \boldsymbol{\theta}$ is the vector of the relative deformation at the joints, namely, $\boldsymbol{\theta}_n - \boldsymbol{\theta}_a$.

The sum of all powers developed by driving devices supplying controlled forces is given by

$$\Pi = \dot{\boldsymbol{\theta}}_a^T \boldsymbol{\tau} + [\dot{\mathbf{c}}]_0^T [\mathbf{f}_s]_0 + [\boldsymbol{\omega}_0]_0^T [\mathbf{n}_s]_0 \qquad (4)$$

where $\boldsymbol{\tau}$ is the vector containing all torques applied by the motors at each joint, and $\mathbf{f}_s$ and $\mathbf{n}_s$ are the forces and moments applied to the spacecraft with devices like thrusters and/or momentum wheels, expressed in the spacecraft frame, $\mathcal{F}_0$. By choosing a set of Euler angles $\boldsymbol{\delta} = [\psi, \phi, \theta]^T$ to describe the base attitude, the base angular velocity $\boldsymbol{\omega}_0$ is expressed as

$$[\boldsymbol{\omega}_0]_0 = \mathbf{S}_0(\boldsymbol{\delta}) \dot{\boldsymbol{\delta}} \qquad (5)$$

where $\dot{\boldsymbol{\delta}}$ are the Euler-angle rates and $\mathbf{S}_0(\boldsymbol{\delta})$ is chosen such that $\boldsymbol{\omega}_0$ is expressed in $\mathcal{F}_0$.

In the realm of the Euler-Lagrange equations, we use $\mathbf{q} = \left[\mathbf{q}_r^T, \boldsymbol{\theta}_a^T\right]^T$, where $\mathbf{q}_r = \left[\mathbf{c}^T, \boldsymbol{\delta}^T, \boldsymbol{\theta}_n^T\right]^T$, as generalized coordinates. Then, applying the Euler-Lagrange equations, the equation of motion can be written as

$$\mathbf{M}\ddot{\mathbf{q}}_r + \mathbf{C}\dot{\mathbf{q}}_r - \mathbf{C}_1\dot{\boldsymbol{\theta}}_a + \mathbf{K}\mathbf{q}_r - \mathbf{K}_1\boldsymbol{\theta}_a + \mathbf{n} = \mathbf{J}_q\boldsymbol{\phi} \quad (6a)$$

$$\mathbf{J}\ddot{\boldsymbol{\theta}}_a - \mathbf{C}_r\dot{\boldsymbol{\theta}}_n + \mathbf{C}_r\dot{\boldsymbol{\theta}}_a - \mathbf{K}_r\boldsymbol{\theta}_n + \mathbf{K}_r\boldsymbol{\theta}_a = \boldsymbol{\tau} \qquad (6b)$$

where $\mathbf{M}$ is a $(6+N) \times (6+N)$ positive-definite mass matrix, $\mathbf{n}$ is a $(6+N)$-dimensional vector containing the nonlinear velocity terms, $\mathbf{J}_q$ is a Jacobian matrix, $\boldsymbol{\phi}$ contains the external forces and moments, and $\mathbf{C}$, $\mathbf{K}$, $\mathbf{C}_1$, $\mathbf{K}_1$ are matrices given as

$$\mathbf{C}_1 = [\mathbf{0}, \mathbf{0}, \mathbf{C}_r]^T, \quad \mathbf{C} = [\mathbf{0}, \mathbf{0}, \mathbf{C}_1] \qquad (7a)$$

$$\mathbf{K}_1 = [\mathbf{0}, \mathbf{0}, \mathbf{K}_r]^T, \quad \mathbf{K} = [\mathbf{0}, \mathbf{0}, \mathbf{K}_1] \qquad (7b)$$

where $\mathbf{0}$ are matrices having appropriate dimensions.

If we assume that joints are blocked in a specific configuration $\boldsymbol{\theta}_a^*$, then $\dot{\boldsymbol{\theta}}_a = \mathbf{0}$ and $\ddot{\boldsymbol{\theta}}_a = \mathbf{0}$. Thus, Eqs.(6a & 6b) become

$$\mathbf{M}\ddot{\mathbf{q}}_r + \mathbf{C}\dot{\mathbf{q}}_r + \mathbf{K}\mathbf{q}_r + \mathbf{n} = \mathbf{J}_q\boldsymbol{\phi} + \mathbf{K}_1\boldsymbol{\theta}_a^* \qquad (8a)$$

$$-\mathbf{C}_r\dot{\boldsymbol{\theta}}_n - \mathbf{K}_r\boldsymbol{\theta}_n + \mathbf{K}_r\boldsymbol{\theta}_a^* = \boldsymbol{\tau} \qquad (8b)$$

Equation (8b) gives the expression for the torques required to brake the joints, and Eq.(8a) represents the dynamics of the system.

2.2 Controller Structure

The technology currently available does not allow the use of proportional thruster valves in space, and thus, classical PD and PID control laws cannot be used; spacecraft attitude and position are controlled by on-off thruster valves, that introduce nonlinearities.

The usual scheme to control a spacecraft with on-off thrusters employs the error phase plane, defined as
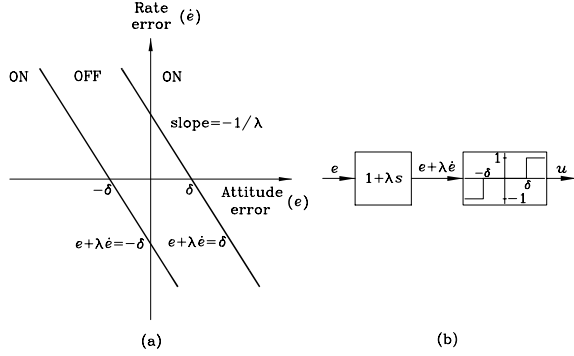
Figure 2: (a) Switching logic in the error phase plane; (b) Controller block.

having the spacecraft attitude error e and error rate $\dot{e}$ as coordinates. The on-and-off switching is determined by switching lines in the phase plane and can become complex, as for example, the phase plane controller of the Space Shuttle [2]. To simplify the switching logic, two switching lines with equations $e + \lambda \dot{e} = \pm \delta$ have been used, as shown in Fig. 2(a). The deadband limits $[-\delta, \delta]$ are determined by attitude limit requirements, while the slope of the switching lines, by the desired rate of convergence towards the equilibrium and by the rate limits. This switching logic can be represented as a relay with a deadband, where the input is $e + \lambda \dot{e}$, the left-hand side of the switching-line equations, see Fig. 2(b).

To compute the input to the controller, the position and the velocity of the base are required and can be obtained from sensors. However, it can happen that only the attitude is available and then, the angular velocity must be estimated. As shown in [4], the use of sensors to obtain the rate of the base may deteriorate the performance of the system due to the high-frequency filtering requirements. Here, we consider that only the attitude is available from sensors, and, hence, to obtain the velocity, estimators are used.

3   Control

In this paper, we assume that the attitude of the spacecraft can be defined by a set of three Euler angles $\boldsymbol{\delta}$. Moreover, we assume that each angle remains small enough to be controlled independently, with the attitude controller presented in Subsection 2.2. The general control system required to control the orientation of a spacecraft in space is thus presented in Fig. 3 where each attitude controller is represented with the block diagram of Fig. 2(b). The plant dynamics is described using the formulation introduced in Subsection 2.1 and is thus represented by the set of highly nonlinear equations (8a). Finally, the state estimator blocks are required to estimate the angular velocity and filter the attitude signals obtained by sensors. Three different
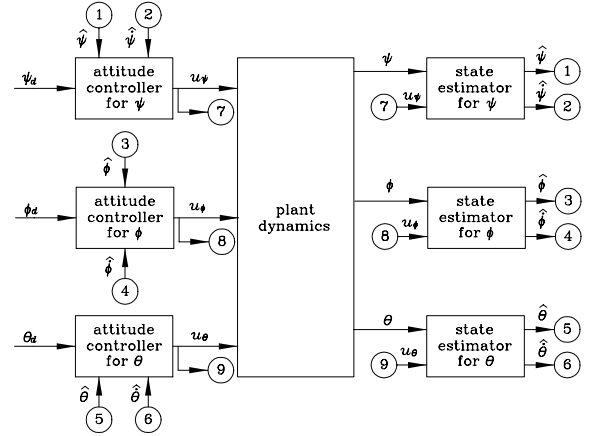

Figure 3: Model with a 3-axis rate estimator and attitude filter.

estimators are presented below and, to draw stability conclusions, the following definition based on the rate of fuel consumption of the system is used. A **stable system (S)** describes a system where the motion reaches a limit cycle similar to the one for a rigid body with a resulting rate of fuel consumption R_f^* smaller than 0.0060 fuel units/s, other cases being **unstable (U)**.

3.1   A Classical Rate Estimator (CRE)

For this estimator, a configuration similar to the one used on the Space Shuttle is employed [2]. A differentiator combined with a second-order filter is used to obtain a velocity estimate, as shown in Fig. 4. The differentiation of a noisy signal is not recommended because it amplifies noise. However, in this case, it is possible to use a scheme where only the flexible part of the motion needs to be differentiated. This means that, at the limit, for a rigid system, no differentiation is necessary. This state estimator can give very good results when flexibility is low. The differentiator-filter is given by $sG_{se}(s)$ where

$$G_{se}(s) = \frac{\omega_{se}^2}{s^2 + 2\zeta_{se}\omega_{se}s + \omega_{se}^2} \qquad (9)$$

The attitude feedback is also low-pass-filtered using a second-order filter represented by $G_f(s)$

$$G_f(s) = \frac{\omega_f^2}{s^2 + 2\zeta_f\omega_f s + \omega_f^2} \qquad (10)$$

For this filter, we use $\zeta_f = 0.707$, and let ω_f free to vary, while, for the differentiator-filter, we use values that correspond to the ones used on the Space Shuttle [2], namely, $\omega_{se} = 0.2513$ rad/s and $\zeta_{se} = 0.707$.

3.2   A Rate Estimator with Linear Compensation (RELC)

In order to improve the performance of the attitude control system, we propose the use of a second-order
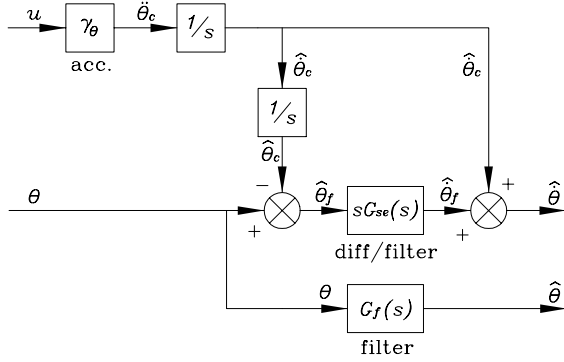
Figure 4: Block diagram for CRE estimator.

compensator of the form

$$G_c(s) = \frac{\omega_p^2(s^2 + 2\zeta_z\omega_z s + \omega_z^2)}{\omega_z^2(s^2 + 2\zeta_p\omega_p s + \omega_p^2)} \qquad (11)$$

The same rate estimator of Fig. 4 is considered, but in this case, both the estimated velocity $\hat{\dot{\theta}}$ and filtered attitude $\hat{\theta}$ are compensated using $G_c(s)$. This compensator was chosen based on the analytical results described in detail in [7].

An important aspect of this estimator is the pole and zero location of the second-order linear compensator $G_c(s)$ of Eq.(11), namely, the determination of ζ_z, ω_z, ζ_p and ω_p. For this task, it is very important to keep in mind that the compensator is cascaded to a second-order filter which is used to eliminate high frequency noise. Therefore, to avoid noise amplification, the zeros of $G_c(s)$ should not be too close to the origin while its poles should not be too far from it. Moreover, by experience, it was observed that the imaginary part of the zeros of $G_c(s)$ should be less than both the imaginary part of the poles of the second-order filter or the imaginary part of the poles of the plant transfer-function. After many trials, a set of guidelines was elaborated to automatically select the poles and zeros of $G_c(s)$. These guidelines do not always lead to the optimal design of the compensator for a particular case, but were found to give good performance in most cases. Another important aspect was the sensitivity of the stability of the system to parameter variations, like those related to the motion of the space manipulator. These guidelines were found to give good reasonable performance for a wide range of motion of the manipulator. Therefore, the imaginary part of the zeros of $G_c(s)$ should be chosen as the minimum value of the imaginary part of the poles of the second-order filters or 75% of the imaginary part of the pole associated with the lowest natural frequency of the system. Moreover, its real part should be chosen as half the higher value between the real part of the poles of $G_f(s)$ and those of $G_{se}(s)$. On the other
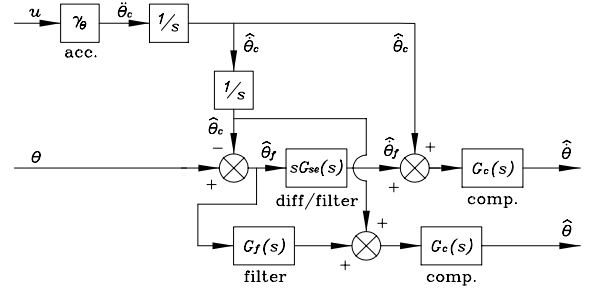
hand, the real part of the poles of $G_c(s)$ should be chosen as the mean value of the real parts of the poles of $G_f(s)$ and $G_{se}(s)$, its imaginary part been null. These guidelines are presented in algorithmic form in [7].

3.3 A New Rate Estimator with Linear Compensation (NRELC)

One way to further improve the performance of the estimator of Fig. 4 is to filter only the "flexible" part of the attitude signal, as is done for the rate estimate $\hat{\dot{\theta}}$. Linear compensation is also considered for this estimator, the above guidelines being also used for the pole and zero determination. This NRELC estimator is presented in Fig. 5.

4 Simulation Results

In this section, the three-flexible-joint manipulator mounted on a six-dof spacecraft of Fig. 6 is considered as the plant. This model has basically the same architecture as the CANADARM/Space Shuttle system when considering only its three first joints. Moreover, in order to choose realistic parameter values for the system, the parameter values of the CANADARM/Space Shuttle system are used, while link flexibility was lumped at the joints and zero joint angles were assumed for its last three joints [8]. This model is described in detail in [7].

Using the *Matlab/Simulink* simulation environment, a parametric study was undertaken to show the performance of the estimators described in Section 3. For this study, the parameters of Table 1 were fixed while λ, the negative inverse of the slope of the switching lines, and ω_f, the cutoff frequency in the second-order filter $G_f(s)$, were given the values $\lambda = 3$ s or $\lambda = 5$ s, and $\omega_f = 0.2513$ rad/s, $\omega_f = 0.47$ rad/s or $\omega_f = 0.6911$ rad/s. Moreover, three typical configurations of the manipulator were considered, namely, $(\theta_1, \theta_3, \theta_5) = (0°, 0°, 0°)$ or $(0°, 135°, -90°)$ or $(120°, 90°, 105°)$, as well as four different payloads, $\beta = 0, 0.1, 0.3,$ or 1.0, where β is the ratio of the mass of the payload to the mass of the spacecraft, $\beta = 0$ and $\beta = 1$ being extreme cases where there is no payload and where the payload mass
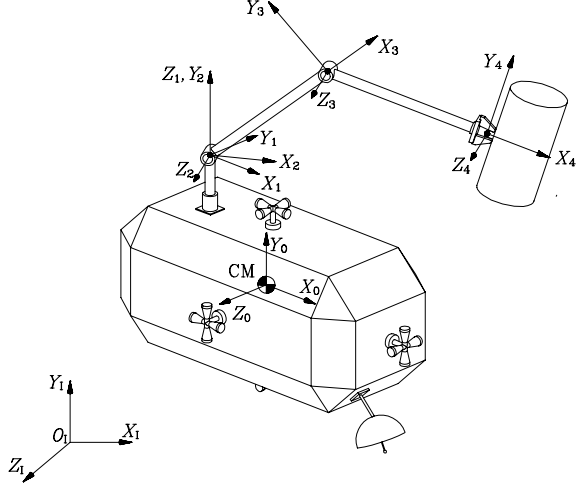
Figure 6: A three-flexible-joint space manipulator

Table 1: Parameter values used for all simulations

δ	γ_θ	τ (s)	ζ_f	ω_{se} (rad/s)	ζ_{se}
$1°$	$0.02°/\text{s}^2$	0.1	0.707	0.2513	0.707

Table 2: Results of the parametric study for $\lambda = 3$ s

ω_f (rad/s)	β	Config. 1			Config. 3			Config. 5		
		1	2	3	1	2	3	1	2	3
0.2513	0.0	U	U	S	U	U	S	U	U	S
	0.1	U	U	S	U	U	U	U	U	S
	0.3	U	U	S	U	U	S	U	U	U
	1.0	U	U	S	U	U	S	U	U	U
0.47	0.0	U	U	S	U	U	S	U	U	S
	0.1	U	U	S	U	U	S	U	U	S
	0.3	U	S	S	U	U	S	U	U	S
	1.0	U	S	S	U	U	S	U	U	S
0.6911	0.0	S	S	S	S	S	S	S	S	S
	0.1	U	S	S	U	S	S	U	S	S
	0.3	U	S	S	U	S	S	U	U	S
	1.0	U	U	S	U	U	S	U	U	S

Table 3: Results of the parametric study for $\lambda = 5$ s

ω_f (rad/s)	β	Config. 1			Config. 3			Config. 5		
		1	2	3	1	2	3	1	2	3
0.2513	0.0	U	U	S	U	U	S	U	U	S
	0.1	U	U	S	U	U	S	U	U	S
	0.3	U	U	S	U	U	S	U	U	S
	1.0	U	U	S	U	S	S	U	U	U
0.47	0.0	S	S	S	S	S	S	S	S	S
	0.1	U	S	S	S	S	S	S	S	S
	0.3	S	S	S	S	S	S	U	S	S
	1.0	U	S	S	U	S	S	U	U	U
0.6911	0.0	S	S	S	S	S	S	S	S	S
	0.1	S	S	S	S	S	S	S	S	S
	0.3	S	S	S	S	S	S	U	S	S
	1.0	U	S	S	U	S	S	U	U	S

is equal to that of the spacecraft. The value $\beta = 0.3$ corresponds to the maximum value that was considered for the CANADARM/Space Shuttle system, while $\beta = 0.1$ corresponds to a more typical payload.

The results of this study are summarized in Tables 2 and 3, respectively for $\lambda = 3$ s and $\lambda = 5$ s, where "U" stands for an unstable system, "S" for a stable system, and 1, 2 and 3 correspond to the CRE, RELC and NRELC estimators, respectively. From this study, it is apparent that the use of linear compensation improves the performance of the CRE estimator. Many simulations that were unstable using the CRE estimator are now stable using the RELC estimator. Moreover, we see that the use of the NRELC estimator further improves the performance of the system. Using this estimator, almost all the cases studied were stable, most of the unstable cases being for $\beta = 1.0$, which corresponds to a very large payload. Moreover, in [7], it is shown using the describing function technique that the RELC estimator is able to eliminate the dynamic interactions that result in large limit cycles. However, it cannot stabilize systems with a diverging motion, as it can be done using the NRELC estimator.

Typical simulation results are displayed in Figs. 7 and 8 for the motion about the Z_0 axis of the spacecraft, as per Fig. 6. The simulations were performed using the parameters of Table 1, with $\lambda = 5$ s, $\omega_f = 0.47$ rad/s, and the configuration $(120°, 90°, 105°)$ of the manipulator with $\beta = 0.3$. An initial error of 0.05 rad was considered for each axis of the spacecraft. The results

of Fig. 7 were obtained using the CRE estimator, while the results of Fig. 8 were obtained using the NRELC estimator. From Fig. 7(a), we see that the controller is not able to bring the spacecraft inside the desired attitude limits and that a large limit cycle is reached. The thrusters then fire on and off continuously, resulting in a high fuel consumption of 1336.6 fuel units, as can be observed in Figs. 7(b) and (c). The resulting rate of fuel consumption is, in this case, 0.8667 fuel units/s. On the other hand, from Fig. 8, we see that the NRELC can bring the same system inside the desired attitude limits without problems. Figure 8(b) shows that only a few firings of the thrusters are required, resulting in a consumption of only 43.0 fuel units for the same 2 000 s run. In this case, the rate of fuel consumption is only 0.0003 fuel units/s. This typical example shows the increase in performance that can be attained using the NRELC estimator.
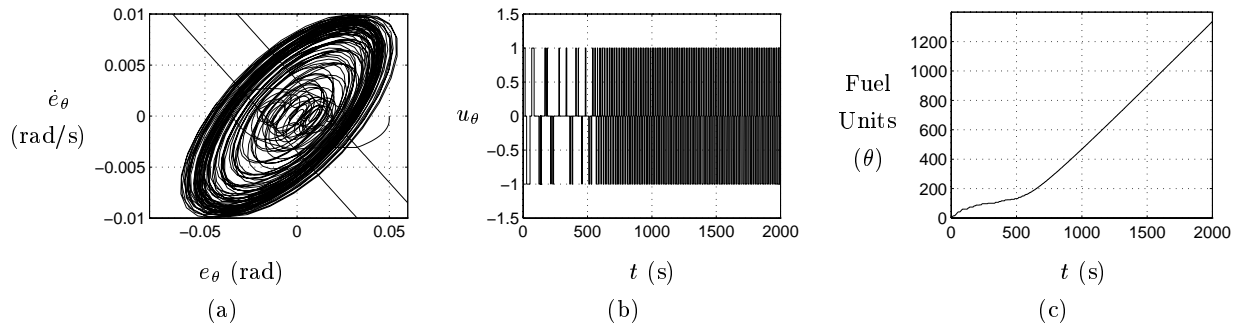
Figure 7: Simulation results for the CRE estimator about the pitch axis: (a) spacecraft error phase plane; (b) thruster command history; and (c) fuel consumption.
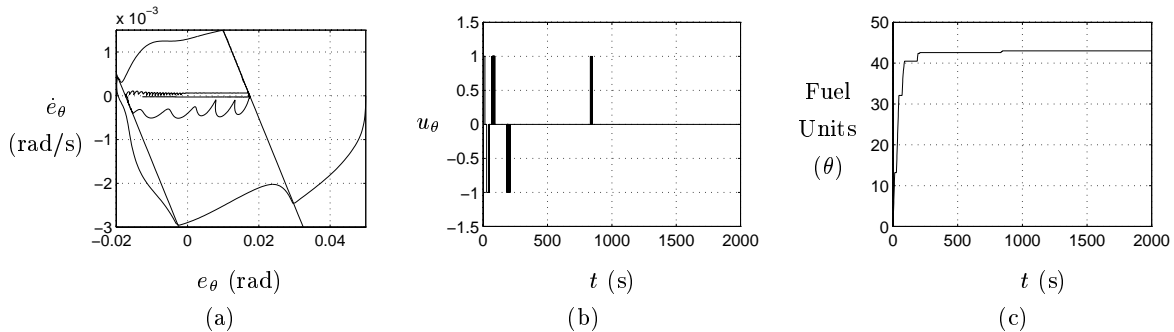

Figure 8: Simulation results for the NRELC estimator about the pitch axis: (a) spacecraft error phase plane; (b) thruster command history; and (c) fuel consumption.

5   Conclusion

This work focused on reducing or eliminating possible dynamic interactions between the attitude controller of a spacecraft and the flexible modes of a space manipulator mounted on it. A three-flexible-joint manipulator mounted on a six-dof spacecraft was used to evaluate three different control/estimation schemes with the help of a parametric study. It was found that the RELC and NRELC estimators can minimize such undesirable dynamic interactions, as well as thruster fuel consumption, thus improving significantly the stability and performance of the system.

Acknowledgements

References

[1] Millar, R. A., and Vigneron, F. R., "Attitude Stability of a Pseudorate Jet-Controlled Flexible Spacecraft," *J. of Guid., Cont., and Dyn.*, Vol. 2, No. 2, 1979, pp. 111–118.

[2] Sackett, L. L., and Kirchwey, C. B., "Dynamic Interaction of the Shuttle On-Orbit Flight Control System with Deployed Flexible Payload," *Proc. of the AIAA Guid. and Cont. Conf.*, San Diego, CA, 1982, pp. 232–245.

[3] Kubiak, E. T., and Martin, M. W., "Minimum Impulse Limit Cycle Design to Compensate for Measurement Uncertainties," *J. of Guid., Cont., and Dyn.*, Vol. 6, No. 6, 1983, pp. 432–435.

[4] Martin, E., Papadopoulos, E., and Angeles, J., "On the Interaction of Flexible Modes and On-off Thrusters in Space Robotic Systems," *Proc. of the 1995 Int. Conf. on Intelligent Robots and Systems, IROS'95*, Pittsburgh, PA, 1995, pp. 65–70.

[5] Martin, E., Papadopoulos, E., and Angeles, J., "Towards Reducing Thruster-Flexibility Interactions in Space Robots," *Proc. of the Eleventh CISM-IFToMM Symposium on Theory and Practice of Robots and Manipulators*, Udine, Italy, 1996, pp. 13–20.

[6] Martin, E., Papadopoulos, E., and Angeles, J., "Control System Design for Reduced Thruster-Flexibility Interactions in Space Robots," *Proc. of the 1996 Canadian Society for Mech.Eng. (CSME) Forum*, Hamilton, Canada, 1996, pp. 125–132.

[7] Martin, E., "Dynamic Interaction of a Space Manipulator with its Base Attitude Controller," Ph.D. Thesis, Dept. of Mech. Eng., McGill University, Montreal, in progress.

[8] Spar Aerospace Ltd., *Payload Deployment and Retrieval System (PDRS) Simulation Database*, SPAR-RMS-TM.2163, Spar Aerospace Ltd, 1996.